MICROEARTHQUAKES AND EFFICIENCY IN CRUSTAL DEFORMATION IN GREECE

Burton,P.W.

School of Environmental Sciences, University of East Anglia, Norwich NR4 7TJ, UK.

A B S T R A C T

Physical properties associated with microearthquake (1.5-4.2 M_L) rupture are examined in three zones in Greece: the Nea Ankhialos fault, Volos; the western Gulf of Corinth, Patras; a microearthquake swarm zone, Pavliani. Average fault radii from the Brune-Madariaga model are 168 m near Volos and about 105 m near Patras and Pavliani, however, average stress drops are 1.2 bar near Volos and 17 bar on the smaller faults at Patras and Pavliani. Log moment scales with log10 stress drop in all zones but source radii only vary slowly. Average strain drops are in the range $2-25*10^{-6}$ but if strain drop localised at asperities is considered values approach crustal strain strength limits of $2*10^{-4}$. Finally, a frictionally controlled process of rupture is considered which suggests that these microearthquakes are efficient converters of small strain into displacement. Tectonic extensional efficiency accompanies low seismic efficiency.

ΜΙΚΡΟΣΕΙΣΜΙΚΟΤΗΤΑ ΚΑΙ ΣΥΝΤΕΛΕΣΤΗΣ ΑΠΟΔΟΣΗΣ ΤΗΣ ΠΑΡΑΜΟΡΦΩΣΗΣ ΤΟΥ ΦΛΟΙΟΥ ΣΤΗΝ ΕΛΛΑΔΑ.

Burton,P.W.

Π Ε Ρ Ι Λ Η Ψ Η

Φυσικές ιδιότητες που αφορούν μικρούς σεισμούς (M_L=1.5-4.2) εξετάζονται σε τρεις ζώνες στην Ελλάδα: στο ρήγμα της Νέας Αγχιάλου (Βόλος), στο δυτικό Κορινθιακό κόλπο (Πάτρα) και στη Παύλιανη, όπου γίνονται σμηνοσειρές. Οι μέσες τιμές των ακτίνων του ρήγματος, όπως υπολογίστηκαν από το μοντέλο Brune-Madariaga, είναι 168m κοντά στο Βόλο και περίπου 105m κοντά στην Πάτρα και στην Παύλιανη. Η μέση πτώση τάσης είναι 1.2 bar κοντά στο Βόλο και 17 bar στα μικρότερα ρήγματα στην Πάτρα και στην Παυλιανή. Ο λογάριθμος της σεισμικής ροπής συσχετίζεται γραμμικά με το λογάριθμο της πτώσης τάσης σε όλες τις ζώνες, αλλά οι ακτίνες των ρηγμάτων μεταβάλλονται λιγότερο. Οι μέσες τιμές της πτώσης της παραμόρφωσης κυμαίνονται μεταξύ 2 και $25*10^{-6}$ αλλά αν θεωρηθεί ότι η πτώση παραμόρφωσης γίνεται μόνο στα εμπόδια, οι τιμές της πλησιάζουν τα όρια αντοχής της παραμόρφωσης του φλοιού ($2*10^{-4}$). Τέλος, εξετάζεται μια διαδικασία διάρρηξης ελεγχόμενη από την τριβή. Σύμφωνα μ' αυτήν, οι μικροσεισμοί μετατρέπουν αποτελεσματικά την μικρή παραμόρφωση σε μετάθεση. Ο συντελεστής απόδοσης σε περιβάλλον εφελκυσμού συνοδεύει χαμηλό συντελεστή σεισμικής απόδοσης.

INTRODUCTION

Microearthquakes are a topic of increasing interest in Greece and have been investigated by a growing number of researchers. Several studies already exist, which without attempting anything like a full list include: King et al.'s (1983) study of tectonics of northwestern Greece; King et al.'s (1985) study of aftershocks associated with the 1981 Corinth earthquakes; Melis et al.'s (1989) study of microearthquakes and seismotectonics in the Gulf of Patras, and Hatzfeld et al.'s (1989) study of subduction beneath the Peloponnesus based on microearthquake focal mechanisms. These works include reference to other studies.

As yet there are few examples of spectral studies of microearthquakes in Greece exploiting the Brune (1970) and Madariaga (1976) model. As portable digital equipment becomes more widely available this field of research is set to grow.

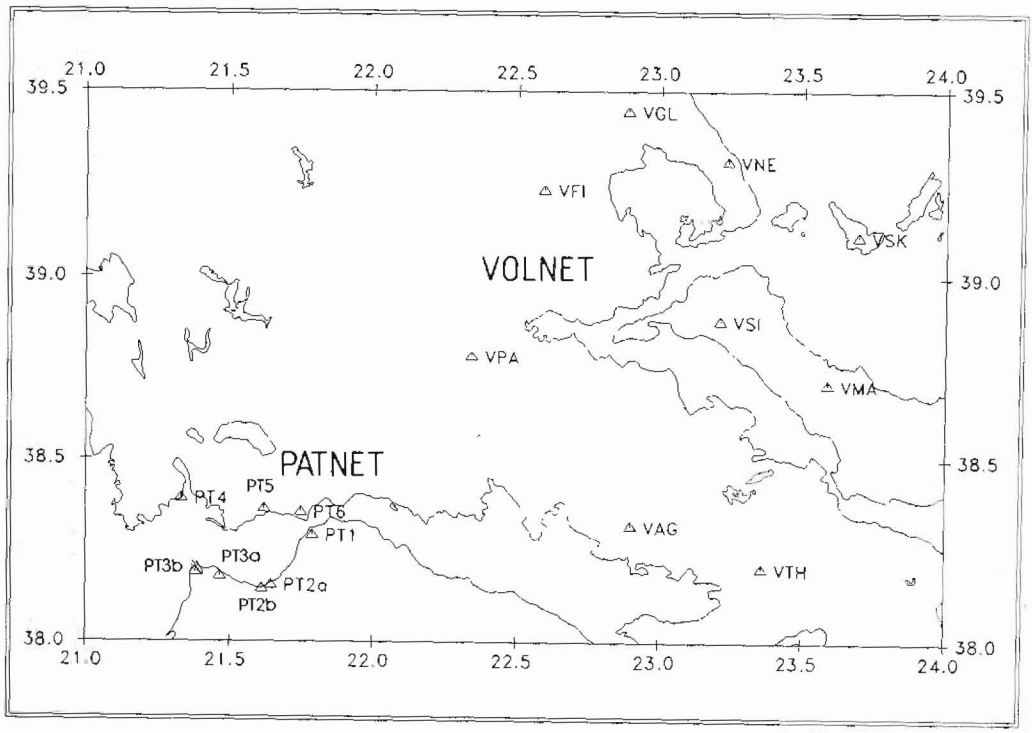

Fig.1. The Volos and Patras seismic networks in central Greece (VOLNET and PATNET). The distance between VSI and VNE is 50 km.

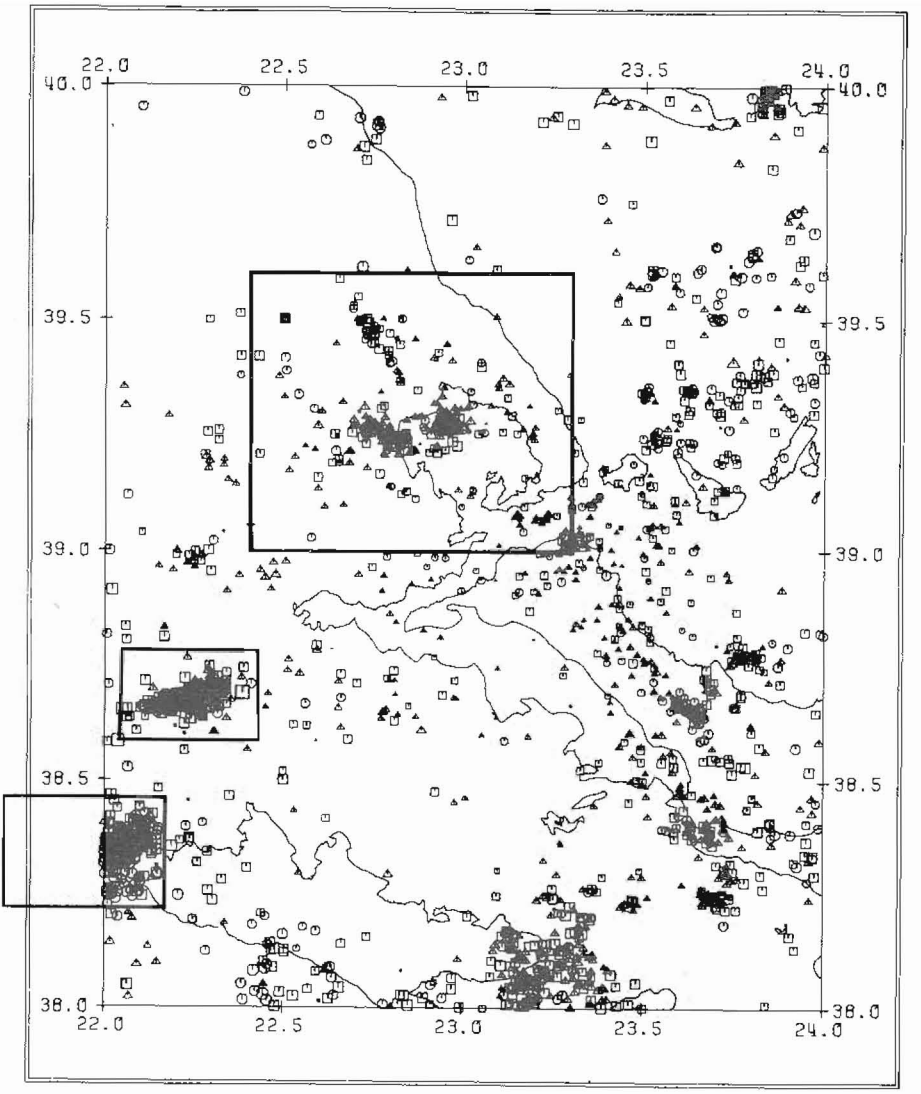

Fig.2. The three study areas. The Nea Ankhialos fault zone, Volos (northern box); the western Gulf of Corinth, Patras (southwestern box); the microearthquake swarm zone, Pavliani (west central box). Microearthquake epicentres recorded by VOLNET in 1983-4.

These techniques allow measurement of physical properties associated with microearthquake rupture, e.g. fault radius, stress drop, coseismic slip. Digital data appropriate to spectral analysis techniques have been obtained from the Volos (Burton et al., 1983-84) and Patras (Melis, 1986) seismic

networks (Figure 1) and results obtained which can be seen in detail in Burton et al. (1991), Abercrombie (1991) and Melis (1992).

The purpose in this paper is firstly to compare results for estimates of physical rupture properties of microearthquakes in three zones in Greece, namely (Fig. 2): the Nea Ankhialos fault, near Volos; the Rio Antirrio and western Gulf of Corinth zone, near Patras; and a zone associated with microearthquake swarm activity, near Pavliani. Such studies have been undertaken in many places outside Greece (for example, see the papers by Archuleta et al., 1982; Gagnepain-Beyneix 1985; Del Pezzo et al., 1987; and papers cited within these). Secondly, consideration will be given to the extent that a frictional controlled process of microearthquake rupture explains the observations, and also to the implications arising from this for crustal deformation in Greek earthquakes.

CALIBRATION OF MAGNITUDES AGAINST NATIONAL AND INTERNATIONAL SCALES

The measured magnitudes, M_L, are in themselves homogeneous and self-consistent although they can be expected to differ systematically from other magnitude determinations made on the same or other earthquakes in the Aegean region. Before attempting to obtain moment-magnitude correlations it is first necessary to determine regional magnitude scale correlations, so

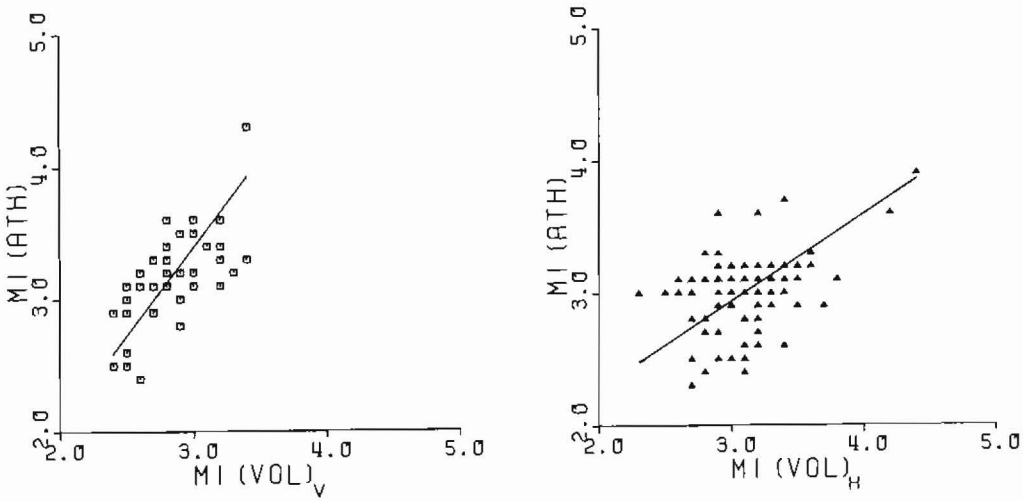

Fig.3. Calibration of local magnitudes $M_L(VOL)_V$ and $M_L(VOL)_H$, estimated using vertical and horizontal components in the Volos seismic network respectively, with the local magnitude $M_L(ATH)$ determined by the National Observatory of Athens.

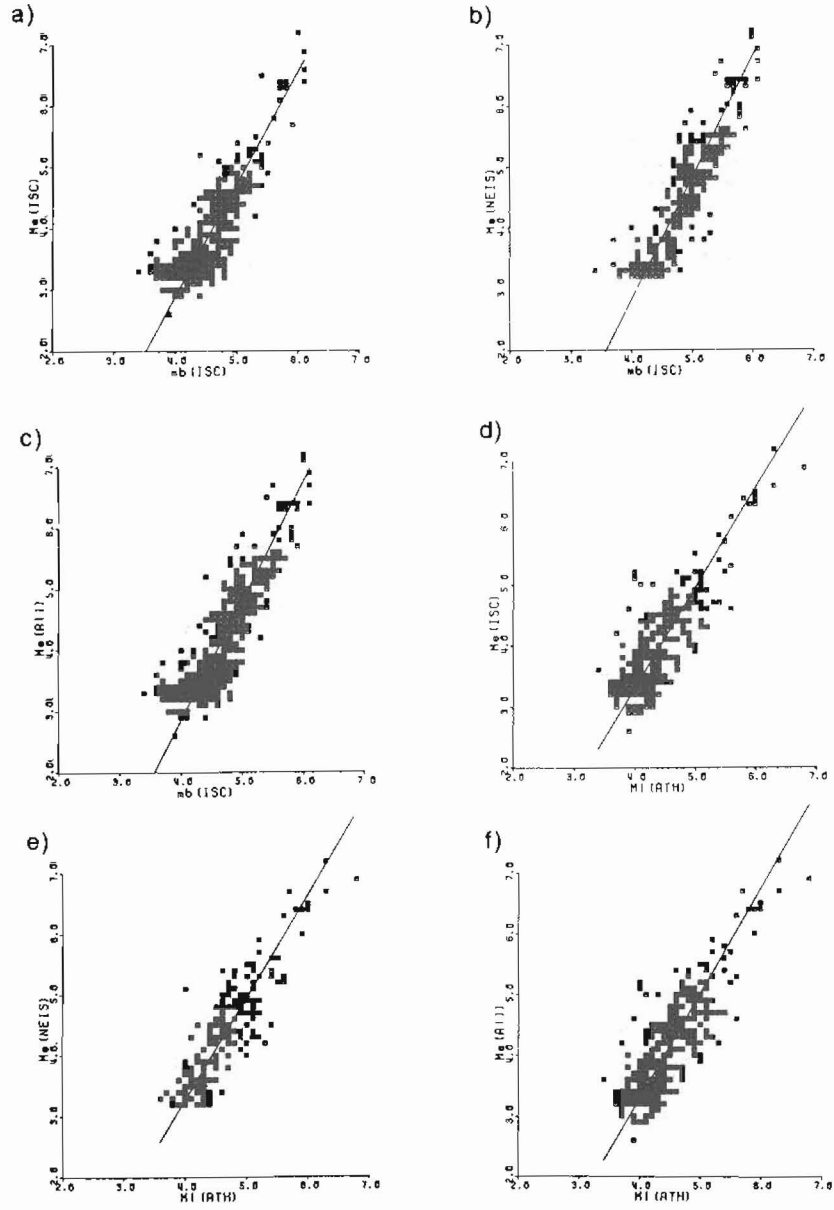

Fig.4. Calibration of local and teleseismic magnitude scales for Greece. International Seismological Centre (ISC) and US National Earthquake Information Service (NEIS) reports provide surface wave and body wave magnitudes: M_s(ISC), M_s(NEIS), m_b(ISC), m_b(NEIS) respectively and combined data sets M_s(ALL) and m_b(ALL). National Observatory of Athens bulletins provide local magnitudes M_L(ATH).

that all magnitudes can be rendered to a standard and accepted baseline. Therefore Richter local magnitudes $M_L(VOL)$ from the VOLNET data for the first six months of 1983 are compared to the corresponding Richter local magnitude $M_L(ATH)$ determined by the National Observatory of Athens (NOA). There are 143 earthquakes of which 95 are "true" Richter magnitudes $M_L(VOL)_H$ determined using horizontal component seismometers. The magnitudes obtained from vertical component seismometers are identified $M_L(VOL)_V$. In the first instance neither $M_L(ATH)$ nor $M_L(VOL)$ is taken as standard and so linear correlation regressions assume equal errors in both magnitude assessments (York, 1966). Regressions are then calculated assuming that the gradient is actually 1.

The data are displayed in Figure 3 corresponding to correlations:

$$M_L(ATH) = (1.35 \pm .15)M_L(VOL)_V + .66\ (\pm .44),\ (N = 48) \quad (1a)$$
$$M_L(ATH) = (0.66 \pm .09)M_L(VOL)_H + .96\ (\pm .28),\ (N = 95) \quad (1b)$$

and assuming the gradient is 1:

$$M_L(ATH) = M_L(VOL)_V + .32\ (\pm .29), \quad (1c)$$
$$M_L(ATH) = M_L(VOL)_H + .09\ (\pm .35) \quad (1d)$$

The simplicity of the assumed gradient of one is preferred, indeed the true Richter magnitudes determined from horizontal components in VOLNET and NOA are, for most practical purposes, the same. Magnitudes measured from vertical component seismometers are systematically smaller by 0.3 than the NOA baseline because horizontal component amplitudes are about twice the vertical component amplitude. Practically all the local magnitudes M_L used in this study correspond to equation 1d and the tiny relative adjustment to the NOA baseline standard.

These regional local magnitude scales can also be correlated with the internationally used M_s and m_b. Magnitude data extracted from the International Seismological Centre (ISC) bulletins and those published by the US National Earthquake Information Service (NEIS) provide the opportunity for comparison with local magnitudes published in the Monthly Bulletins of the National Observatory of Athens. The regressions obtained from the data illustrated in Figure 4 are:

$$M_s(ISC) = (1.85 \pm .06)m_b(ISC) - 4.51\ (\pm .27), \quad (2a)$$
$$M_s(NEIS) = (1.95 \pm .06)m_b(ISC) - 5.04\ (\pm .31), \quad (2b)$$
$$M_s(ALL) = (1.96 \pm .05)m_b(ISC) - 4.98\ (\pm .24), \quad (2c)$$

and secondly,

$$M_s(ISC) = (1.64 \pm .05)M_L(ATH) - 3.25\ (\pm .23), \quad (3a)$$
$$M_s(NEIS) = (1.69 \pm .05)M_L(ATH) - 3.49\ (\pm .28), \quad (3b)$$
$$M_s(ALL) = (1.70 \pm .05)M_L(ATH) - 3.59\ (\pm .22), \quad (3c)$$

It is difficult to see any evidence for a break of gradient in Figures 4a-c of the kind noted by Kiratzi and Papazachos (1984) around 4.3 m_b and the M_s and M_L correlations appear linear in Figures 4d-f throughout the plotted magnitude range. The equations 2-3 provide good calibration of the local magnitudes

in Greece against the internationally accepted scale values.

MEASUREMENT OF SOURCE PARAMETERS OF MICROEARTHQUAKES IN CENTRAL GREECE

The intention is to examine the physical rupture properties of micro-earthquakes in three seismogenic zones. The principal zone is Volos following the work of Burton et al. (1991); Patras and Pavliani are included to a lesser extent in the light of Melis (1992) and Melis et al. (1993a,b). Physical quantification of microfaulting, which can be assessed through spectral analysis, includes several useful parameters, viz. seismic moment, fault radius, average slip, average stress drop and the associated strain drop.

The displacement spectrum of ground motion caused by an earthquake can be modelled simply by a low frequency asymptotic displacement, Ω_o, intersecting a high frequency decay at the corner frequency f_c Hz. The velocity of rupture across a fault of finite size controls the corner frequency value and leads to a finite duration to rupture; this model is attributable to and well described by Brune (1970) and Madariaga (1976). The analysis which follows in this paper usually only considers P-waves. The necessary equations to determine the parameters of interest are firstly:

$$M_o = 4\pi\rho\alpha^3 R\Omega_o/0.85 \qquad (4a)$$

and

$$f_c = 0.32\beta/r, \qquad (4b)$$

in which spectral measurements of the low-frequency asymptote and the corner frequency are used to measure seismic moment, M_o, and source radius, r. Reasonable estimates of density, ρ, P-wave velocity, α, hypocentral distance, R, and a composite allowance of 0.85 for reflection at the free-surface and radiation pattern at the source are also necessary. The static definition of seismic moment gives

$$M_o = \mu As \qquad (5)$$

where μ is the shear modulus, A is the fault area and s the average slip on the fault. Shear velocity at the source is taken to be the velocity at the focal depth in the velocity-depth model used to locate the hypocentres (see Burton et al., 1991). This is preferred to a half-space value covering all focal depths. The compressional-to-shear wave velocity ratio of 1.78 adopted by King et al. (1983) for Greece is used. A circular fault model is assumed following Kanamori and Anderson (1975) and the remaining physical rupture properties which are estimated are:

$$s = M_o/\pi r^2\mu \qquad (6a)$$
$$\Delta\sigma = 7M_o/16r^3 \qquad (6b)$$
$$\Delta e = M_o/\pi r^3\mu \qquad (6c)$$

where $\Delta\sigma$ and Δe are stress and strain drops respectively. The source radius r appears in many of these equations, either as r, r^2 or the cubic r^3, and is itself determined from the corner frequency using Madariaga's (1976) results which assume a rupture velocity at the source of 0.9β (β km s^{-1} is the shear wave velocity). The adopted values of density and shear modulus in equations 4-6 are $\rho = 2.7$ gm cm^{-3} and $\mu = 3*10^{10}$ N m^{-2}.

At first sight the windowing used to extract the P-wave or other phase of interest, from the seismogram, appears to be a critical decision and the variety of conventions used by different workers is large (e.g. Street et al., 1975; Sereno and Bratt, 1988; Burton and Marrow, 1989; Archuleta et al., 1982; Gagnepain-Beyneix, 1985; Del Pezzo et al., 1987). Secondly, there has been intense debate about the use of attenuation or Q corrections to allow for absorption along the propagation path (e.g. Mueller and Cranswick 1985; Brune et al., 1986; Fletcher et al., 1986; Anderson, 1986). After extensive trials we have reached the conclusion that windowing, although of interest when there are mixed crustal phases in the coda, is not critical. Attenuation corrections usually appear to have indiscernible effect on the corner frequency and a small percentage change in the asymptotic displacement, weighted against this is the reading uncertainty in Ω_o which amounts to a factor of 2 or 3 and is equivalent to 0.3 or 0.5 in M_L. What does appear useful in phase identification is the inspection of deconvolved displacement seismograms prior to windowing and spectral analysis (Abercrombie, 1991). The interested reader is referred to the extensive trials and discussions in Burton et al. (1991), Abercrombie (1991) and Melis (1992). The conventions adopted allow for: cosine tapering by 5% both at the start and finish of the window; noise removal by subtraction of Fourier harmonic amplitudes in the frequency domain for an equivalent length noise window; seismograph response correction; eye-ball fit of the model to the log displacement spectrum. The two lines fitted by eye are not drawn in as envelopes to all excursions of the spectra but follow an eye-ball estimate of the mean trend and therefore go through the larger spectral oscillations. Errors in reading values of Ω_o and corner frequency from log displacement spectral graphs are themselves log normally distributed and so average seismic moments, $<M_o>$, and uncertainties, etc. are determined from means of logarithmic values (Archuleta et al., 1982; Gagnepain-Beyneix, 1984), for example:

$$<M_o> = antilog\ (\frac{1}{N}\sum \log M_{oi}) \qquad (7)$$

when averaged over results from N stations. These random reading errors create typical errors of order a factor 2-3 in M_o and r, 4 in s and about 6-8 in $\Delta\sigma$ and Δe, but usually we examine graphs of the log of these quantities in which the scatter is much less.

MICROEARTHQUAKE SOURCE PARAMETERS: PARAMETER VALUES AND RELATIONSHIPS IN THREE REGIONS IN EASTERN AND CENTRAL GREECE

This section will now describe the results for physical parameters describing source rupture of microearthquakes in three regions in eastern and central Greece: Volos, Patras and Pavliani. The emphasis will be on results from Volos.

Nea Ankhialos fault, Volos

Microearthquakes recorded during 1983-84 follow three main shocks which occurred during 1980 (Papazachos et al., 1983) with parameters:

1980 July 9 02 hr 10 min 19 s 39.252°N 23.008°E h=13 km 5.6 M_s
02 hr 11 min 57 s 39.283°N 23.110°E h= 9 km 6.5 M_s
02 hr 35 min 52 s 39.190°N 22.733°E h=12 km 6.0 M_s

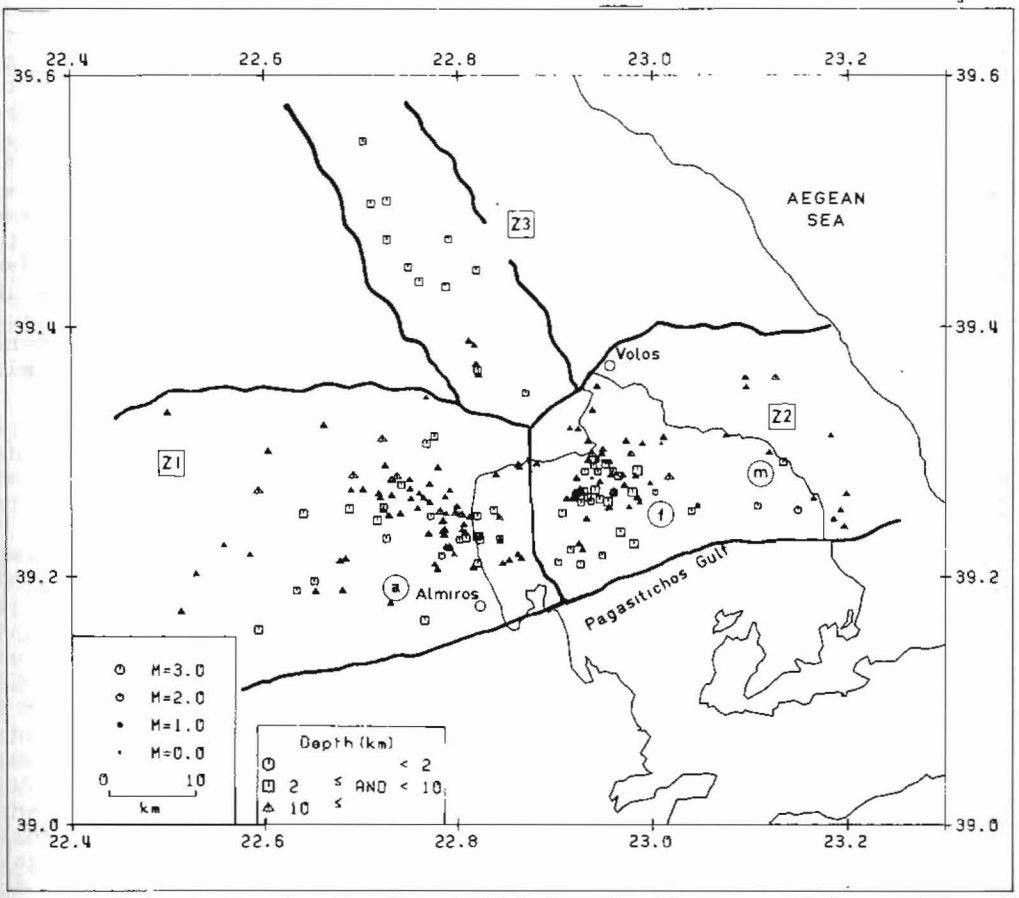

Fig.5. Seismicity in the Nea Ankhialos fault zone, Volos. Z1: Nea Ankhialos fault, western segment; Z2: Nea Ankhialos fault, eastern segment; Z3: region north of Nea Ankhialos fault. Foreshock, main shock and aftershock in the 1980 July 9 earthquake sequence are represented by f, m and a.

and are associated with the Nea Ankhialos fault zone, south of the city of Volos. The microearthquakes cluster in the Pagasitichos Gulf, the Almiros Basin and the region north of Volos forming the three zones indicated in Figure 5. Results for the three zones are compared in detail in Burton et al. (1991); the third zone is the more anomalous whereas there are only minor differences between Z1 and Z2 and these two zones may be regarded as western and eastern segments of the Nea Ankhialos fault zone.

Originally, 96 microearthquakes were sampled from the seismicity illustrated in Figure 5 but this number reduces to 78 applying the criteria that each earthquake should be observed with at least five phase data. Pairs of $<R\Omega_o>$ and $<f_c>$ from which estimates of M_o, etc. are made are shown in Figure 6a. Corner frequencies in Figure 6a span 3.5-13 Hz with typical values around 7 Hz. The two lines have a slope of -3 expected for constant stress drop earthquakes (Aki 1967) and these do not appear to be representative of the data. The more rigorous constraint that only those earthquakes generating five or more pairs of spectral measurements of corner frequency and long period asymptote are retained produces the final set of results for 58 earthquakes, with 25 in the western segment and 23 in the eastern segment of the fault. This emphasises the nearest stations surrounding the Pagasitichos Gulf and Almiros Gulf. This final set of earthquakes produces results for magnitude, seismic moment in N m, average fault radius in m, average stress drop in bars and average slip in mm on an assumed circular fault. A summary of these results is listed in Table 1 and this provides the basis for Figures 6c-f. An appreciation of uncertainties in these results is important and microearthquake 1,1 of Table 1 provides an example. Standard deviation ranges around the geometric means in M_o, r, $\Delta\sigma$ and s obtained from logarithmic standard deviations for earthquake 1,1 parameters are:

$$<M_o> = 4.2 \,^{+7.7}_{-2.7} \times 10^{12} \; N\,m$$

$$<r> = 233 \,^{+147}_{-91} \; m$$

$$<\Delta\sigma> = 1.4 \,^{+16}_{-1.3} \; bar$$

$$<s> = 0.8 \,^{+3.1}_{-0.8} \; mm$$

The 1.4 bar stress drop for earthquake 1,1 is the mean within the one standard deviation range 0.1-17 bar. This illustrates why some rupture parameters in their conventional representation can

only be known to an order of magnitude.

The variation of seismic moment with depth (Figure 6b) is scattered rather than systematic although there is a slight tendency to reach maximum values in the top half of the crust; the other variations in Figures 6c-f are much more revealing. Inspection of all four Figures 6c-f reveals that the eastern segment of the Nea Ankhialos fault is relatively heterogeneous in its parameters in comparison to the western segment, but the contrasts are not great and allow combination of both segments to represent the fault as a whole. The northern zone is relatively anomalous and off the main fault trend (detailed comparison of parameters of the three zones is discussed in Burton et al. 1991).

Seismic moment and magnitude: the data in Figure 6c can be represented by the standard equation:

$$\log M_o = A + BM_L \qquad (8)$$

where typical values of B are around 1 for microearthquakes (B ≈ 1.5 for intermediate sized earthquakes, Kanamori and Anderson, 1975). Double error regression on $\log\langle M_o\rangle$ and M_L pairs, assuming equal errors in both, for the Nea Ankhialos fault produces:

$$\log\langle M_o\rangle = (10.1 \pm 0.2) + (0.9 \pm 0.1)M_L, \ (N=48, \ cc=0.85) \qquad (9)$$

with a high correlation coefficient cc = 0.85. Abercrombie (1991) examined 17 microearthquakes on the Nea Ankhialos fault, scattered over both segments, 11 in the North Aegean and 12 in the Gulf of Corinth, and independently arrived at:

$$\log\langle M_o\rangle = (10.5 \pm 0.1) + (0.8 \pm 0.05)M_L, \ (N=40, \ cc=0.94) \qquad (10)$$

with an even higher correlation coefficient of 0.94. It is clear that the Nea Ankhialos fault exhibits a systematic relationship between $\langle M_o\rangle$ and M_L along its east-west extent to a high degree of correlation, along with many other microearthquakes in Greece.

Seismic moment and fault radius: The parallel reference lines in Figure 6d represent three different levels of average stress drop. Geometrical similarity or scaling of fault size for fault rupture across a continuum of energy release levels is often held to be synonymous with a constant stress drop. The data in Figure 6d are consistent with a typical average stress drop of around 1 bar but overall the observed correlation between seismic moment and average fault radius is considerably weaker than between moment and average slip (see below) and moment and magnitude (above). The eastern segment has radii in the range 86-214 m and the western segment has the range 128-304 m. The average fault radii averaged over the whole fault (Z1 + Z2) is 168 m. It appears that fault radius is more-or-less constant for this size of earthquake, or only varying slowly. This suggests that these microearthquakes are characterised by some crustal 'grain size', and as events get smaller (in moment) the dominant way to reduce the energy release is to have less average slip.

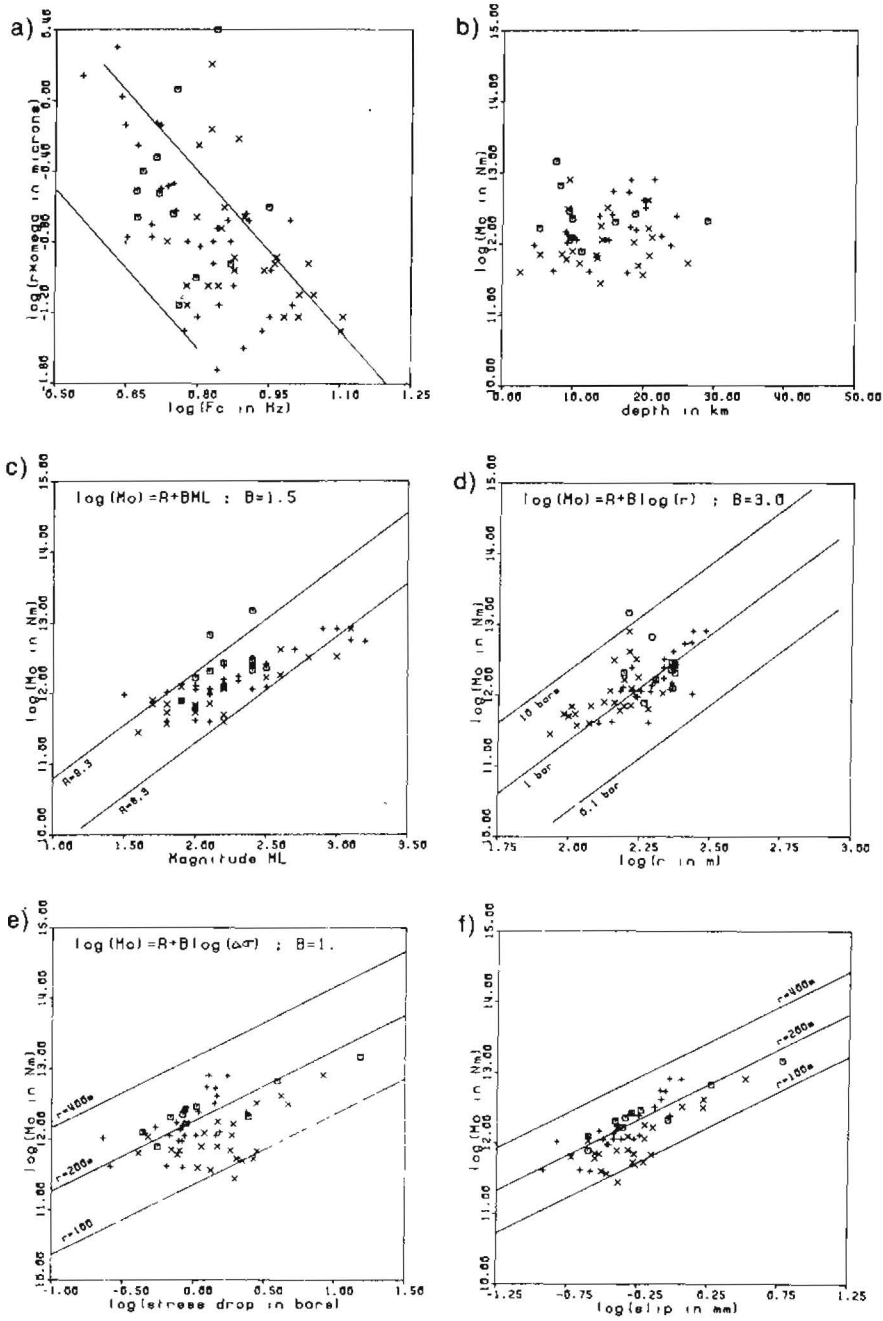

Fig.6. Nea Ankhialos fault zone. (a) Ω_o corrected for epicentral distance paired with corner frequency f_c. (b)-(f) Seismic moment and focal depth, local magnitude, average fault radius, average stress drop and average coseismic slip. Symbols represent zones: Z1 = +, Z2 = x, Z3 = ⊡ .

Table 1. Seismotectonic source parameters of microearthquakes in the Nea Ankhialos fault complex. N: the number of spectra from which corner frequency were measured.

Event Zone, no.	M_L	M_o (10^{12} N m)	Radius (m)	Stress drop (bar)	Slip (mm)	N
Nea Ankhialos fault, western segment						
1,1	2.7	4.2	232.6	1.4	0.82	6
1,2	2.9	8.2	303.8	1.3	0.94	8
1,4	3.2	5.4	254.8	1.4	0.88	7
1,6	2.4	1.2	151.7	1.4	0.53	7
1,7	2.5	1.2	227.1	0.5	0.25	8
1,10	2.4	2.5	215.7	1.1	0.57	6
1,12	3.0	8.1	273.8	1.7	1.14	7
1,14	1.5	1.0	171.3	0.8	0.35	5
1,15	2.0	1.1	179.3	0.9	0.38	6
1,16	2.4	1.1	194.2	0.7	0.32	8
1,19	2.2	2.5	166.0	2.4	0.95	5
1,20	2.0	0.4	141.7	0.7	0.22	6
1,22	2.1	1.0	174.5	0.8	0.34	7
1,25	1.8	1.1	272.5	0.2	0.15	6
1,26	2.3	1.5	230.3	0.5	0.30	7
1,27	1.8	0.4	190.9	0.3	0.12	6
1,29	2.0	1.3	154.9	1.5	0.58	5
1,30	2.5	2.6	236.5	0.9	0.50	8
1,31	2.1	0.4	127.7	0.8	0.26	5
1,32	2.1	1.2	169.2	1.0	0.43	8
1,33	2.2	1.6	202.1	0.8	0.41	6
1,34	2.4	3.3	216.3	1.4	0.74	7
1,35	3.1	5.6	270.8	1.2	0.81	6
1,36	2.3	1.7	215.8	0.8	0.40	8
1,37	2.2	1.4	195.6	0.8	0.38	7
Nea Ankhialos fault, eastern segment						
2,3	1.9	0.8	144.9	1.1	0.40	6
2,4	1.7	0.1	71.1	1.1	0.19	5
2,6	2.6	4.1	163.3	4.2	1.65	8
2,7	2.0	0.6	190.5	0.4	0.19	5
2,8	2.1	1.1	214.0	0.5	0.25	5
2,9	3.1	8.1	162.5	8.3	3.25	8
2,12	2.8	3.2	143.9	4.7	1.63	10
2,14	2.5	1.7	156.6	1.9	0.72	9
2,15	3.0	3.3	172.7	2.8	1.16	8
2,16	1.6	0.3	85.7	2.0	0.41	5
2,17	2.2	0.5	99.7	2.2	0.54	8
2,18	2.0	0.5	95.8	2.7	0.62	6
2,19	2.2	0.4	117.8	1.1	0.31	8
2,20	1.8	0.1	97.5	0.7	0.16	5
2,23	1.7	0.8	133.3	1.5	0.48	6
2,24	2.0	0.7	102.3	2.8	0.70	6
2,25	2.0	0.6	151.4	0.8	0.28	7

2,26	1.8	0.7	119.5	1.8	0.53	6
2,28	2.2	1.2	139.6	1.9	0.63	7
2,29	1.8	0.5	105.4	2.0	0.52	7
2,30	2.1	0.7	165.2	0.7	0.28	8
2,31	1.8	0.4	106.7	1.3	0.34	8
2,32	1.7	0.7	156.1	0.8	0.30	6
2,33	2.6	1.8	175.2	1.5	0.63	7
2,34	1.9	1.2	166.0	1.2	0.48	5
2,35	2.1	0.5	116.2	1.4	0.40	6
Region north of Nea Ankhialos fault						
3,4	2.4	2.9	230.2	1.1	0.59	5
3,5	2.1	6.7	195.8	3.9	1.86	8
3,6	2.0	1.7	202.3	0.9	0.44	6
3,7	2.4	2.1	155.6	2.4	0.92	5
3,8	2.4	14.7	161.8	15.2	5.97	7
3,13	2.5	2.3	228.9	0.8	0.46	6
3,14	1.9	0.8	184.1	0.6	0.25	5
3,22	2.2	1.3	232.4	0.4	0.25	7
3,23	2.2	2.7	237.2	0.9	0.51	6
3,24	2.1	2.1	236.3	0.7	0.39	7

Seismic moment and stress drop: The parallel reference lines in Figure 6e are drawn for three reference average source radii. There is an observable correlation between moment and average stress drop and a consistent pattern emerges which is more compatible with a constant radius than constant average stress drop. Correlation coefficients are of order cc ≈ 0.5 although Abercrombie's (1991) values reach 0.93.

Seismic moment and fault slip: The reference lines in Figure 6f are again drawn for three reference average source radii. The static definition of seismic moment in equation 5 extended to slip on a circular fault in equation 6a implies a linear relationship between log<s> and log<M_o> for faults of approximately constant radius. Correlation is clearly observable in Figure 6f. Values of cc are 0.87 and 0.81 if the western and eastern segments are taken separately and drop to cc = 0.73 when the whole Nea Ankhialos fault is taken:

$$\log \langle M_o \rangle = (12.6 \pm 0.1) + (1.6 \pm 0.2)s, \ (N=48, \ cc=0.73), \quad (11)$$

the reduction in cc reflecting the slightly different properties in western and eastern fault segments. Abercrombie's (1991) analysis produces correlations as high as cc = 0.97. Inspection of Figure 6b, however, does suggest differences between eastern and western segments. The data for the western segment cluster around the 200 m reference line whereas for the eastern segment nearly all the data fall between the 100 m and 200 m lines. These differences exist even though the range of seismic moments is almost identical being $0.4 - 8.2*10^{12}$ N m compared to $0.3 - 8.1*10^{12}$ N m.

In summary these data suggest that microearthquakes in the eastern segment have smaller fault areas and larger average

slips, a factor of about 3, than in the western segment, and overall the eastern segment appears to be the slightly more heterogeneous segment. Source radius is approximately constant in each segment, or varying very slowly with seismic moment. Gross average physical properties of the microearthquakes on the Nea Ankhialos fault are summarised in Table 2.

Table 2. Averages and ranges of the seismotectonic source parameters in three zones.

	Nea Ankhialos Fault, Volos	Patras Zone	Pavliani Fault	Unit
Range of focal depths	2.5-26.3	0.7-36.3	5.6-23.3	km
Range of local magnitudes	1.5-3.2	1.8-3.9	1.8-4.2	M_L
Range of seismic moments	0.28-8.16	0.3-45.7	0.9-94.9	10^{12} Nm
Range of slip on faults	0.12-3.25	0.36-41.2	1.85-32.2	mm
Range of fault radii	86-304	48-310	65-226	m
Range of stress drops	0.23-8.26	0.7-175	5.0-103	bar
Average focal depth	14.7	9.65	13.2	km
Average local magnitude	2.24	2.72	2.49	M_L
Average seismic moment	1.30	4.34	4.85	10^{12} Nm
Average slip on fault	0.51	4.52	4.43	mm
Average fault radius	168	103	108	m
Average stress drop	1.19	17.2	17.0	bar
Average strain drop	1.71	24.8	23.1	10^{-6}
Typical asperity radius	5.80	13.5	14.1	m

Strain drop: The gross averages in Table 2 can be used to estimate representative strain drop, $\langle\langle\Delta e\rangle\rangle$, defined as

$$\langle\langle\Delta e\rangle\rangle = \langle\langle s\rangle\rangle/\langle\langle r\rangle\rangle\pi^{1/2} \qquad (12)$$

Gross average slip and fault radii in the western and eastern segments are 0.47 mm and 202 m, and 0.54 mm and 138 m respectively, leading to mean values of representative strain drop of $1.3*10^{-6}$ and $2.2*10^{-6}$ respectively. For the Nea Ankhialos fault as a whole the value is $\langle\langle\Delta e\rangle\rangle = 1.7*10^{-6}$. Compared to plate boundary seismicity where $\Delta e \approx 10^{-4}$ (Kanamori,1977) these values are small and accompanied by tiny average slip values. Jackson et al. (1982) obtained strain drops of order $5*10^{-5}$ during the major earthquakes in Corinth in 1981. Strain drops in the microearthquakes are nevertheless seen to be about one order

of magnitude less than in major Greek earthquakes although a standard deviation range on strain drop encompasses a factor of about 15.

Apparent stress: corroborative evidence for average stress drop

The most striking results in the above observations are that the average fault radii are approximately constant with seismic moment while average stress drops are not, gross typical values being summarised in Table 2. However, a fundamental difficulty is that much of the analysis is model dependent, i.e. the Brune and Madariaga models require measurement of a corner frequency which may be perturbed by f_{max} (Hanks 1982) and other factors. Any suspected perturbation to the corner frequency is problematic because the average fault radius, r, is inversely proportional to corner frequency and the derived quantity average stress drop is itself sensitive to r^3. Apparent stress, σ_{ap}, has been suggested by Wyss (1970) as a model independent parameter related to stress drop and interpreted by Savage and Wood (1971) as "stress associated with radiation resistance". If the final stress equals the frictional stress then it is given by:

$$\sigma_{ap} = \eta(\sigma_1+\sigma_2)/2 = \mu E/M_o \qquad (13)$$

where σ_1 and σ_2 are initial and final stresses, η is efficiency and E is the radiated energy. Snoke et al. (1983) demonstrate the useful inequality

$$\sigma_{ap} \leq \Delta\sigma/2 \qquad (14)$$

where the equality only applies if no new crack surfaces are generated during rupture and the final stress is equal to the frictional stress. The problem is thus to calculate the radiated seismic energy, E. This is proportional to the area under the velocity-squared seismogram and for a P-wave, Boatwright (1980) gives:

$$E_p = \frac{2\pi\rho\alpha R^2 I_{pz}}{\cos(i)(F_s U_{\phi\theta})^2} \qquad (15)$$

where I_{pz} is the integral for the vertical P-wave component, i the angle of incidence, and $(F_s U_{\phi\theta})$ allows for the free surface reflection and radiation pattern. Boatwright gives similar expressions for the three components of S-wave motion and so E_s and hence $E=E_p+E_s$ can be calculated. Abercrombie (1991) has developed this procedure for 40 selected microearthquakes distributed amongst Volos, the North Aegean and the Gulf of Corinth. Figure 7 is a sample of Abercrombie's results. In this example log moment scales with both log stress drop and with log apparent stress, correlation coefficients exceeding 0.9 and 0.8 respectively. The net result is that log stress drop scales with log apparent stress (cc = .72, or 0.59 if the gradient is fixed as 1.0):

$$\log\Delta o = \log\sigma_{ap} - 0.12(\pm 0.06) \qquad (16)$$

The ensuing conclusion is that use of the model independent stress corroborates the results detailed above from the Brune-Madariaga model dependent analysis. Abercrombie's result allows us to proceed to analyses for Patras and Pavliani with greater confidence.

An indication of possible systematic errors in moment (or Ω_o) and fault radius (or f_c) can be deduced. Equation 16 can be rewritten as $\sigma_{ap} = 1.32\Delta\sigma$ whereas equation 14 suggests that the constant should be 0.5 or less, apparently the constant is a factor 2.64 greater than the accepted maximum value. Combining equations 6b and 13 gives

$$\sigma_{ap}/\Delta\sigma = 16\mu Er^3/7M^2_o \qquad (17)$$

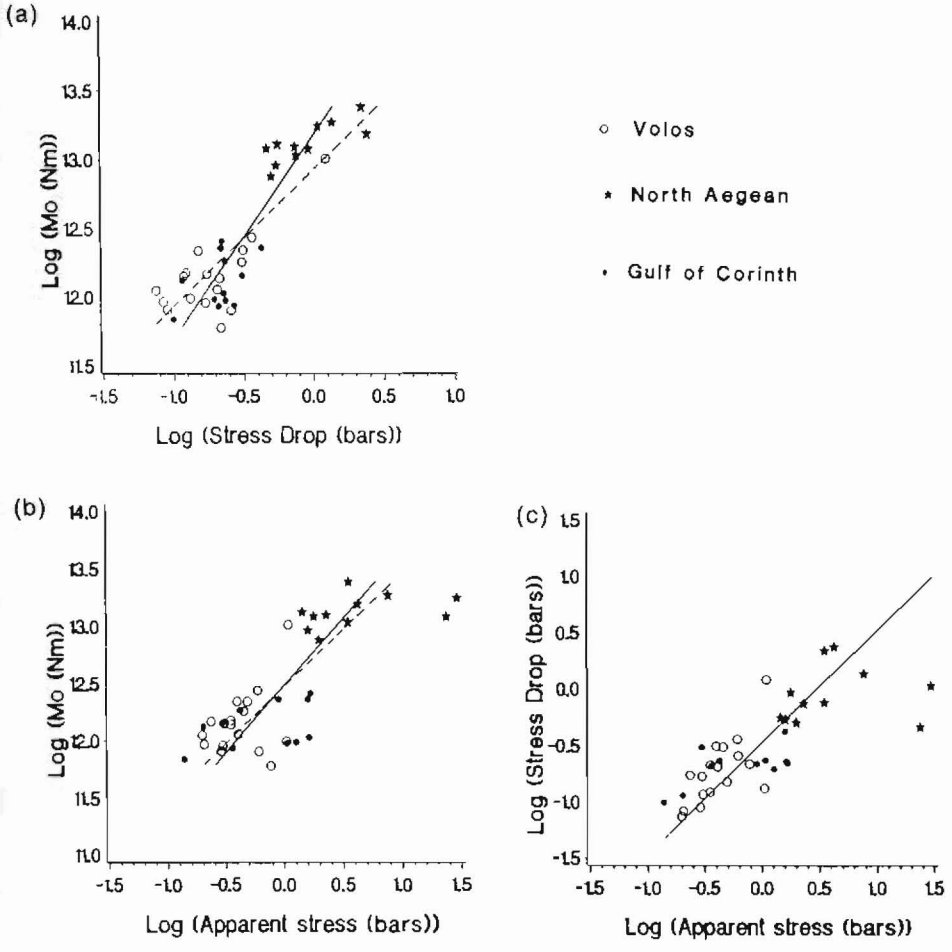

Fig.7. Seismic moment, average stress drop and apparent stress. Solid lines in a) and b) are regressions with variable gradient and dashed lines in a) and b) and solid line in c) have gradient of 1 (adapted from Abercrombie, 1991).

The ratio can be high if estimates of apparent stress are high or stress drops are low, in both cases this may correspond to underestimates of moment (or low Ω_o). If this is the total source of error then moment or measured values of Ω_o are about 38% lower than they ought to be. Systematic error might also arise if model dependent stress drops alone are too low, resulting from too high estimates of r^3 (or low f_c). If this is the total source of error then measured values of f_c are about 28% lower than they ought to be. Such an error in moment or Ω_o corresponds to about -0.2 in magnitude i.e. these are fairly small and typical errors overall.

Patras zone

108 earthquakes recorded by either the Volos network or the Patras network (Figure 1) and located in the south west zone shown as a box in Figure 2 provide the results for this section. These 108 well located earthquakes are mostly confined within the western Corinth Gulf, the Rio Antirrio narrows, with more epicentres northwards towards Trikhonis, and this number reduces to 94 events which are fully spectrally analysed. The details of this analysis are given in full by Melis (1992) and summarised by Melis et al. (1993b). This zone is known to be tectonically complex (Brooks et al. 1988; Melis et al. 1989). The averages and ranges of the physical source parameters resulting from the spectral analysis etc. are summarised in Table 2. The most vital aspects of these data for our present purpose are summarised in Figure 8.

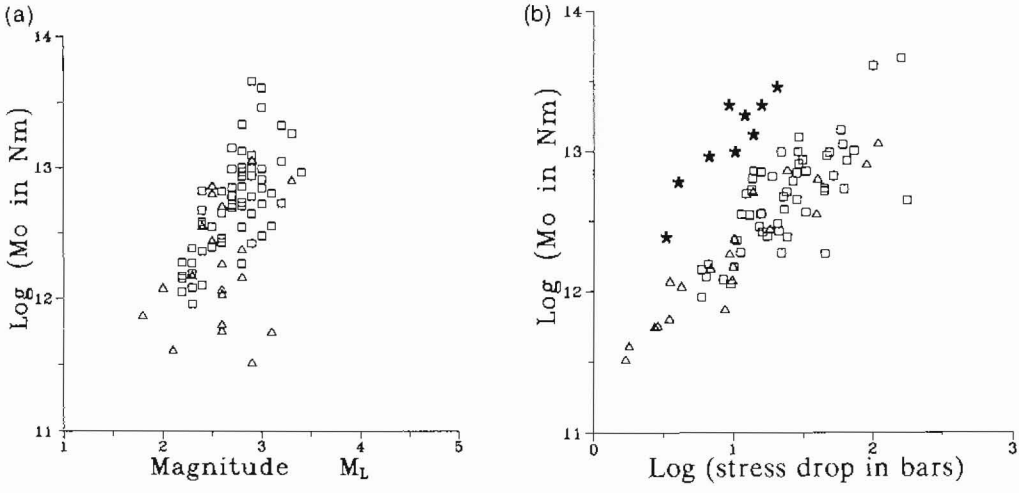

Fig.8. Rio Antirrio and western Gulf of Corinth zone, Patras. Seismic moment and a) local magnitude, b) average stress drop. The star symbol in b) identifies the most anomalous values in the western Gulf of Corinth (adapted from Melis, 1992).

Figure 8a shows poorer correlation between log moment and magnitude in the Patras zone than was the case in the Volos zone.

This is readily interpretable as arising from the relatively complicated tectonics near Patras compared to the more readily understood tectonics associated with the Nea Ankhialos fault. Subdividing the Patras zone into subzones provides only debatable improvement (Melis 1992). Figure 8b demonstrates scaling between log moment and log stress drop although there is substantial scatter. The most anomalous data in Figure 8b (indicated by stars) all locate in the western Corinth Gulf and this region requires more detailed study.

Ranges and gross averages for seismic moment, fault radius, stress drop and average slip etc. for the Patras zone earthquakes are summarised in Table 2. Although the range of moments is quite large, source radii are nearly constant or conceivably slowly varying. There is a clear contrast to the Nea Ankhialos fault, Volos. Average magnitudes and moments analysed in the Patras zone are larger than for the Volos zone, however the average fault radius is less (103 m against 168 m) and average stress drops and slips are greater (17.2 bar against 1.2 bar and 4.5 mm against 0.5 mm). The significance of this will be discussed later.

Pavliani zone

For this zone 70 earthquakes recorded by the Volos network and located in the central zone shown as a box in Figure 2 provide the results. The seismicity in this zone is spatially well constrained and gives an immediate appearance similar to aftershocks on a large fault. Most of the seismicity depicted in Figure 2 occurred as two periods of swarm activity during April and September 1983. The analysis of these swarms and interpretation as a pseudo-fault is given in detail by Melis (1992) and Melis et al. (1993a). The data necessary to our

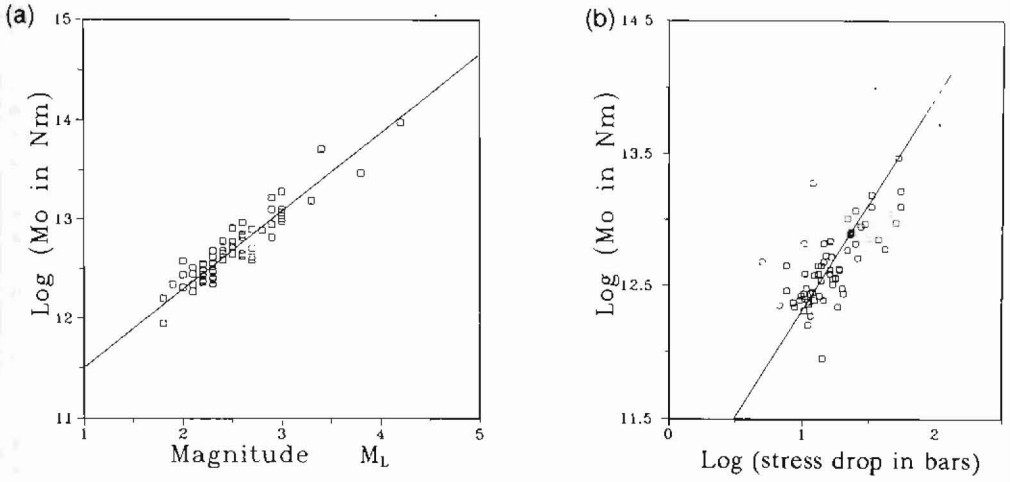

Fig.9. Microearthquake swarm zone, Pavliani. Seismic moment and a) local magnitude, b) average stress drop (adapted from Melis, 1992).

present purpose are summarised in Figure 9 and arise from 66 earthquakes for which the spectral analysis was complete. Ranges and gross averages for seismic moment etc. are again summarised in Table 2.

Inspection of Figure 9a shows excellent correlation between log moment and magnitude with a correlation coefficient of 0.93. The regression equation of Melis (1992) is compatible with equations 9 and 10, being:

$$\log M_0 = (10.7 \pm 0.1) + (0.79 \pm 0.04) M_L, \quad (N=66, cc=0.93) \qquad (18)$$

Figure 9b shows good correlation (cc=0.72) between log moment and log stress drop. The entire data set appears homogeneous compared to Patras underlining the apparent tectonic simplicity in the Pavliani zone.

Ranges and gross averages for seismic moment, fault radius, stress drop and average slip in the Pavliani zone (see Table 2) are very similar to those observed in Patras, although being more homogeneous, and show the same differences with respect to the Volos zone. For example, average magnitudes and moments analysed at Pavliani are higher than in Volos but average fault radius is less, 108 m, and average slip, 4.43 mm, and stress drops, 17.0 bar, are greater.

ASPERITY AND FRICTIONAL CONTROL IN CRUSTAL DEFORMATION

Average stress drops in microearthquakes on the Nea Ankhialos fault in the Volos zone have a mean of 1.2 bar and in the Patras and Pavliani zones, which themselves show tectonic differences, the mean is 17 bar. In all cases these values are substantially lower than the expected strengths of rocks which are of order kilobars in the laboratory. We also observe seismic moment scaling with stress drop whereas source radii either scale very slowly or are nearly constant. How can these observations be interpreted?

Aki's (1984) asperity modelling allows us to explore fault heterogeneity. The measured stress drops are averages over the fault rupture surface and locally can be substantially higher at an asperity than elsewhere. Stress drop $\langle \Delta\sigma_a \rangle$ at an asperity on the rupture surface can be related to stress drop averaged over all the rupture surface, which is the measured value $\langle \Delta\sigma \rangle$, by the fault area A to asperity area A_a ratio. In Table 2 gross averages over many earthquakes are considered and so $\langle \Delta\sigma \rangle$ is better replaced by $\langle\langle \Delta\sigma \rangle\rangle$ and Madariaga's (1979) relation becomes:

$$\langle\langle \Delta\sigma_a \rangle\rangle = \langle\langle \Delta\sigma \rangle\rangle \langle\langle A \rangle\rangle / \langle\langle A_a \rangle\rangle \qquad (19)$$

Take the limit in which the observed gross average stress drop occurs at a single asperity and amounts to 1 kbar. The resulting gross average asperity radii for Volos, Patras and Pavliani zones are 5.8 m, 13.5 m and 14.1 m respectively. However, note that the largest gross average fault radius (168 m) is in the Volos zone. On this simple model of stress drop concentrated at the asperity with aseismic slip elsewhere on the rupture surface, the

relative percentages of fault associated with the dominant asperity are 0.1%, 1.7% and 1.7% respectively; that associated with the Nea Ankhialos fault being over an order of magnitude less than in the other two zones. The equivalent strains if concentrated at the dominant asperity are $5*10^{-5}$, $1.9*10^{-4}$ and $1.8*10^{-4}$ respectively. Tsubois (1956) suggests $2*10^{-4}$ as the limit to strain strength in the crust.

We can now investigate these average stress drops in terms of frictional control of the rupture process. Initial stress and final stress following slip and the static frictional stress σ_f on the rupture surface will be governed by the physical conditions which prevail on the fault. Tectonic stress on a fault can be expected to substantially influence the gross average stress drop and the areal extent of asperities associated with in situ high local stress drop. Average stress $\sigma_{av} = (\sigma_1 + \sigma_2)/2$ and this scaled by the seismic efficiency η becomes the apparent stress or apparent driving force on the fault (see equation 13 and Savage and Wood 1971). Seismic efficiency is influenced by shear strength or frictional stress on the fault and is $\eta = (\sigma_{av} - \sigma_f)/\sigma_{av}$. Equation 13 can be recast in terms of seismic energy radiated and work done on the fault through $E = \eta\sigma_{av} A_s$ or $E = \sigma_{ap} A_s$. Kanamori and Anderson (1975) invoke a fractional stress drop $E = \Delta_o/\sigma_1$ which is related to seismic efficiency through $\eta = E/(2-E)$.

Normal behaviour suggests that $\sigma_1 > \sigma_f > \sigma_2$ with dynamic frictional stress arresting the continuation of slip. In large earthquakes Kanamori and Anderson conclude $\sigma_f \approx \sigma_2$ because they observe $\sigma_{ap} \approx \Delta\sigma/2$; this is compatible with our error of observation discussed above and so we make the same assumption for the observed microearthquakes. Table 3 illustrates typical values of the more important parameters, and how they vary, for the two specific cases of average stress drops of 1.2 bar and 17 bar, corresponding to the Nea Ankhialos fault, Volos and the Patras and Pavliani zones respectively.

Table 3. Frictional control of rupture. Fractional stress drop E, efficiency η, fractional frictional stress σ_f/σ_1, for microearthquakes in Greece.

			Nea Ankhialos fault, Volos ($\Delta\sigma$= 1.2 bar)		Patras zone and Pavliani fault ($\Delta\sigma$ = 17 bar)	
E	η	σ_f/σ_1	σ_1	σ_f	σ_1	σ_f
1.0	1.0	0	1.2	0.0	17	0
0.5	0.33	0.5	2.4	1.2	34	17
0.1	0.053	0.9	12	10.8	170	153
0.05	0.026	0.95	24	22.8	340	323
0.01	0.0050	0.99	120	118.8	1700	1683
0.005	0.0025	0.995	240	238.8	3400	3383
0.001	0.00050	0.999	1200	1198.8	17000	16983
0.0005	0.00025	0.9995	2400	2398.8		
0.0001	0.00005	0.9999	12000	11998.8		

Table 3 is consistent with the view that friction plays a significant role during rupture of these microearthquakes. Average stress drops of 1.2 bar and 17 bar, leading to a residual shear stress of 1 kbar (Sibson, 1982), by interpolation in the Table, imply efficiencies of $6*10^{-4}$ and $8.4*10^{-3}$, respectively. These low seismic efficiencies are accompanied by high frictional fractional stress values. At 9 km depth (the focal depth of the 1980 July 9 magnitude 6.5 M_s main shock in Volos) the overburden pressure amounts to approximately 2.7 kbar. High values of frictional fractional stress prevail in Table 3 and so if σ_1 and σ_f are similar to the overburden pressure then kbar stress levels are quite rapidly approached with depth in the crust.

Table 3 supports the conclusion that if stress of the order of kilobars is needed for rupture then σ_f approaches σ_1 . The in situ tectonic stress need only be slightly greater than the restraining force of static fraction on the fault for rupture to take place. In general $\sigma_1 > \sigma_f > \sigma_2$ and usually we accept $\sigma_1 > \sigma_f \approx \sigma_2$ but in the present case we have $\sigma_1 \approx \sigma_f \approx \sigma_2$. This is compatible with small average slips over relatively large fault areas. The important implication is that the stress need go only slightly higher than the restraining frictional force for faulting or rupture to take place. This is particularly true on the Nea Ankhialos fault but also true in the Patras and Pavliani zones, and appears to be representative of the extensional tectonic regime in Greece.

The range of focal depths in Table 2 extend throughout most of the crust suggesting that the process which controls microearthquake rupture is prevalent at all these depths. This requires some explanation. The friction σ_f or frictional shear force τ on a fault is determined by the normal stress σ_n through:

$$\tau = c\sigma_n \qquad (20)$$

and c is a constant, the coefficient of friction. Typically $\tau=0.85\sigma_n$ up to 2 kbar and $\tau = 0.5 + 0.6\sigma_n$ for normal stress in the range 2-20 kbar at room temperature (Byerlee, 1978). Such frictional stresses are much less than rock strength up to the brittle-ductile transition deep in the crust when the distinction between fracture and friction becomes meaningless. Rock strengths are highly temperature dependent whereas Byerlee's frictional law is largely independent of temperature up to quite high temperatures (e.g. Stesky et al., 1974). Consistency in the frictional process up to temperatures of about 400°C is supportive of frictional control of rupture in microearthquakes for most of the crustal seismicity properties summarised in Table 2. Secondly, it should be noted that the differential stresses required to overcome fault friction and initiate slip on thrust, strike-slip and normal faults are in the ratio 4:1.6:1 (Sibson, 1974). Therefore frictional sliding will be favoured to greater depth in an extensional regime than in any other. Thirdly, pore water pressures p kbar may substantially reduce the normal stress σ_n to an effective stress σ_n -p and high pore-fluid pressures of order 95% of the lithostatic pressure may be reached (e.g. Rutter, 1972). This also creates an argument for low effective restraining frictional forces maintaining seismicity in the deeper crust.

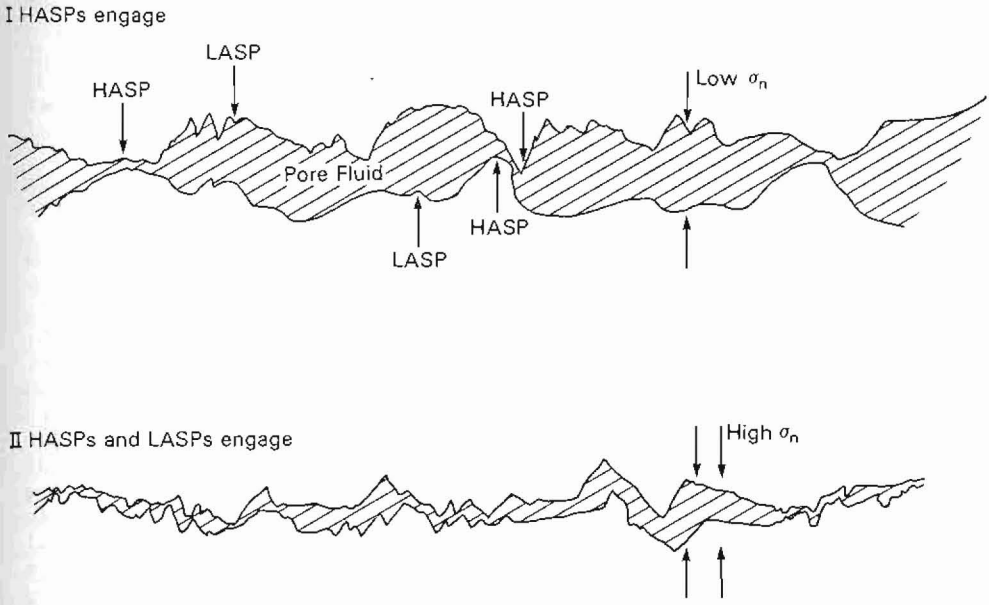

Fig.10. Model of frictional control of rupture. Case I only high asperity profiles (HASPs) interact under low effective normal stress, σ_n. Seismically inefficient but extensionally efficient microearthquakes result on this fault as the HASPs judder over or through each other. Apparent average stress and strain drops are low although they will be high locally at the HASPs. Case II both HASPs and LASPs (low asperity profiles) interact at high effective normal stress. This fault is reluctant to convert low apparent average strain to coseismic deformation.

The main features of Tables 2 and 3 can now be interpreted. Coseismic slip is taking place at a lowered effective σ_n. This slip need not shear through many asperities because this would imply high stress drop averaged over the fault, but it can shear through the high asperity profiles (HASPs) with high local stress drop while gliding aseismically over the majority of roughnesses or low asperity profiles (LASPs) without stress drop. If the sliding displacements were large then this could be described as asperity glide (large displacement against friction), however, they are tiny and it is better described as asperity judder (small displacement against friction). The case when only HASPs engage is Case I in Figure 10. It has low asperity to fault radius ratio and low asperity density. This is the case in our microearthquakes. For comparison, the case when HASPs and LASPs engage under high σ_n is shown schematically as Case II. Case II will be accompanied by high average stress drop and high seismic efficiency, however, it will be a fault which is reluctant to convert strain to coseismic displacement. Scholz (1988) suggests

that fault roughness is fractal with a characteristic length forming between asperities when two surfaces are brought together under normal load. The mated contact area will vary with effective normal stress. In the extreme case of one dominant asperity, which for these microearthquakes occupies only 1% of the fault rupture area, this characteristic length may be almost synonymous with the approximately constant fault radii and of order 100 m.

The frictional process on the faults will allow either aseismic glide over the LASPs or shear interaction with HASPs in stick-slip fashion - effectively steady aseismic glide over a relatively large area interrupted by stick on HASPs and subsequent coseismic slip which amounts to a tiny slip or judder averaged over a relatively large microfault of order 10^4 m^2. Asperity interaction is highly localised within the fault. However, this amounts to the fault restraining frictional force, locally of kbar order, although the fault averaged stress drop is tiny. This is another characteristic of asperity judder: it is the continual transformation of small strain into displacement. The average strain drops are also small being of order 10^{-6} - 10^{-5} for the microearthquakes although locally they approach crustal strain strength values of $2*10^{-4}$. This is an extensionally efficient earthquake regime. This frictional process is characterised by a near equality of tectonic stress and frictional stress during faulting and is accompanied by inefficient seismic release of small average stress drop. These earthquakes are extensionally efficient, even more so in the Volos than the Patras and Pavliani zones.

CONCLUSIONS

Microearthquakes in three areas of Greece have been examined in some detail. Local magnitudes for microearthquakes in the Nea Ankhialos fault zone near Volos are very similar to those determined by the National Observatory of Athens, being about 0.1 less. In turn these local magnitudes have been correlated with international scales using surface wave magnitudes, etc. determined by the International Seismological Centre.

The range of magnitudes examined overall spans 1.5 to 4.2 M_L with corresponding seismic moments 0.3 to $95*10^{12}$ Nm. Spectral analysis using the Brune-Madariaga model gives similar results for the Patras and Pavliani zones with gross average values for fault radii about 105 m, average slip about 4.5 mm, average stress drop about 17 bar and average strain drop about $24*10^{-6}$. On the other hand, the corresponding values for the Nea Ankhialos fault, where magnitudes and moments analysed are on average less, show larger fault radii (168 m) and smaller slip (0.5 mm), stress drop (1.2 bar) and strain drop ($1.7*10^{-6}$).

In all three zones a correlation is observed between log moment and magnitude and log moment and log stress drop. This scaling is weakest in the Patras zone which is the most complex tectonically, whereas these correlations are good in the other two zones of relative tectonic simplicity where one fault system appears to dominate each zone. In all cases the fault radii appear to scale very slowly with seismic moment and are almost

constant being of order 100 m. A difficulty in the analysis is that it is dependent on the Brune-Madariaga model and results might be systematically in error if, for example, the spectral corner frequency is perturbed. This concern is overcome using Abercrombie's (1991) observations which show log stress drop scaling with log apparent stress for Greek microearthquakes, apparent stress being a model independent parameter similar to stress drop. This gives confidence in the results in all three zones.

The summary of rupture characteristics in Tables 2 and 3 lend themselves to a frictional interpretation of the rupture process. In situ tectonic stress grows with time to exceed the static frictional stress on the fault, leading to dynamic slip and stress drop to lower stress. Fault frictional stress and final stress are taken to be nearly equal and the unusual but important situation arises in which all three appear to be very nearly equal. The stresses will obey the hierarchy $\sigma_1 > \sigma_f > \sigma_2$ but with $\sigma_1 \approx \sigma_f \approx \sigma_2$. If shear stress only marginally exceeds the static frictional forces then faulting will occur. Strain drops in the microearthquakes are low being of order $10^{-6} - 10^{-5}$, although locally at asperities, particularly in Patras and Pavliani, Tsubois' crustal strain strength limit of $2*10^{-4}$ is approached. These microearthquakes are efficient converters of small strain into displacement. Tectonic extensional efficiency accompanies low seismic efficiency.

The example of a single asperity on a fault is the limit to low asperity density. This is generalised in Figure 10 to a model of high asperity profiles (HASPs) in which the HASPs engage under lowered normal stress to create local contact points for friction. Small strain is translated to displacement as the HASPs judder over each other. If normal stress increases across the fault other asperities will interact until the LASPs engage and lock the fault more tightly. This second case will produce a more brittle fault which is reluctant to convert strain to coseismic displacement.

ACKNOWLEDGEMENTS

I have to thank many people for assistance and discussion over the years in which I have been involved studying seismicity in Greece. I am particularly grateful to my colleague Kostas Makropoulos and also R. E. Abercrombie, N. S. Melis (including their diagrams) and R. W. McGonigle, I. G. Main and M. E. A. Ritchie. There are many omitted but they should know that I am glad of their help both in the field and in the laboratory.

The Patras seismic network was supported by the Universities of Cardiff and Patras, and the Volos seismic network by the British Geological Survey and the University of Athens, including support from the Natural Environment Research Council. Continuing support for part of this work is provided by NERC Grant GRq/1005.

REFERENCES

Abercrombie,R., (1991). Earthquake rupture dynamics and neotectonics in the Aegean region. Ph.D. Thesis, P.R.I.S., University of Reading.

Aki,K., (1967). Scaling law of seismic spectrum. J. Geophys. Res., 72, 1217-1231.

Anderson,J.G., (1986). Implication of attenuation for studies of the earthquake source. In: S. Das, J. Boatwright and C. H. Scholz (eds.), Earthquake Source Mechanics, Geophysical Monograph 37, Maurice Ewing 6, 311-318.

Archuleta,R.J., Cranswick,E., Mueller,C. and Spudick,P., (1982). Source parameters of the 1980 Mammoth Lakes, California, earthquake sequence. J. Geophys. Res., 87, 4595-4607.

Boatwright,J., (1980). A spectral theory for circular seismic sources: simple estimates of source dimension, dynamic stress drop and radiated energy. Bull. seism. Soc. Am., 70, 1-27.

Brooks,M., Clews,J.E., Melis,N.S. and Underhill,J.R., (1988). Structural development of Neogene basins in western Greece. Basin Res., 1, 129-138.

Brune,J., (1970). Tectonic stress and the spectra of seismic shear waves from earthquakes. J. Geophys. Res., 75, 4997-5009.

Brune,J.N., Fletcher,J., Vernon,F., Haar,L., Hanks,T. and Berger,J., (1986). Low stress-drop earthquakes in the light of new data from the Anza, California telemetered digital array. In: S. Das, J. Boatwright and C. H. Scholz (eds.), Earthquake Source Mechanics, Geophysical Monograph 37, Maurice Ewing 6, 237-245.

Burton,P.W., Makropoulos,K.C., McGonigle,R.W., Ritchie,M.E.A., Main,I.G., Kouskouna,V. and Drakopoulos,J., (1991). Contemporary seismicity on the Nea Ankhialos fault: Fault parameters of major and minor earthquakes, Brit. Geol. Surv., Seismology Series, Report WL/91/29, 106 pages.

Burton,P.W. and Marrow,P.C., (1989). Seismic hazard and earthquake source parameters in the North Sea. In: S. Gregersen and P. W. Basham (eds.), Earthquakes at North-Atlantic Passive Margins: Neotectonics and Postglacial Rebound, Kluwer Academic Publishers, 633-664.

Burton,P.W., McGonigle,R.W., Ritchie,M.E.A., Raines,M.G., Morgan,S.N., Makropoulos,K.C. and Agellis,S., (1983-4). VOLNET Station Bulletins, Jan. 1983 - Dec. 1984, Brit. Geol. Survey & Univ. of Athens, joint open file reports.

Byerlee,J.D., (1978). Friction of rocks. Pure appl. Geophys., 116, 615-626.

Del Pezzo,E., De Natale,G., Martini,M. and Zollo,G., (1987). Source parameters of micro-earthquakes at Phlegraean Fields (Southern Italy) volcanic area. Physics Earth Plan. Ints., 47, 25-42.

Fletcher,J.B., Haar,L.C., Vernon,F.L., Brune,J.N., Hanks,T.C. and Berger,J., (1986). The effect of attenuation on the scaling of source parameters for earthquakes at Anza, California. In: S. Das, J. Boatwright and C. H. Scholz (eds.), Earthquake Source Mechanics, Geophysical Monograph 37, Maurice Ewing 6, 331-338.

Gagnepain-Beyneix,J., (1985). Variation of source parameters of small western Pyrenean earthquakes and their relation to main shock occurrence. Annales Geophysicae, 3, 381-394.
Hanks,T.C., (1982). f_{max}. Bull. seism. Soc. Am., 72, 1867-1879.
Jackson,J.A., Gagnepain,J., Houseman,G., King,G.C.P., Papadimitriou,P., Soufleris,C. and Virieux,J., (1982). Seismicity, normal faulting, and the geomorphological development of the Gulf of Corinth (Greece): the Corinth earthquakes of February and March 1981. Earth Planet Sci. Lett., 57, 377-397.
Kanamori,H., (1977). The energy release in great earthquakes. J. Geophys. Res., 82, 2981-2987.
Kanamori,H. and Anderson,D.L., (1975). Theoretical basis for some empirical relations in seismology. Bull. seism. Soc. Am., 65, 1073-1095.
King,G.C.P., Tselentis,A., Gomberg,J., Molnar,P., Roecker,S.W., Sinvhal,H., Soufleris,C. and Stock,J.M., (1983). Microearthquake seismicity and active tectonics of northwestern Greece. Earth Plan. Sci. Letters, 66, 279-288.
King,G.C.P., Ouyang,Z.X., Papadimitriou,P., Deschamps,A., Gagnepain,J., Houseman,G., Jackson,J.A., Soufleris,C. and Virieux,J., (1985). The evolution of the Gulf of Corinth (Greece): an aftershock study of the 1981 earthquakes. Geophys. J. R. astr. Soc., 80, 677-693.
Kiratzi,A.A. and Papazachos,B.C., (1984). Magnitude scales for earthquakes in Greece. Bull. seis. Soc. Am., 74, 969-985.
Madariaga,R., (1976). Dynamics of an expanding circular fault. Bull. seis. Soc. Am., 66, 639-666.
Melis,N.S., Brooks,M. and Pearce,R.G., (1989). A microearthquake study in the Gulf of Patras region, western Greece, and its seismotectonic interpretation. Geophys. J. R. astr. Soc., 98, 515-524.
Melis,N.S., (1992). Earthquake hazard and crustal deformation in central Greece. Ph.D. thesis, University of Cardiff.
Melis,N.S., Brooks,M. and Burton,P.W., (1993a). Coseismic crustal deformation from microseismicity and "neotectonic" investigations in the Kaloscopi-Pavliani district, central Greece. 2nd Congress of the Hellenic Geophysical Union, 1993 May 5-7, Florina, Greece.
Melis,N.S., Burton,P.W. and Brooks,M., (1993b). Seismic hazard, microseismicity and coseismic crustal deformation in the Patras region, central Greece. 2nd Congress of the Hellenic Geophysical Union, 1993 May 5-7, Florina, Greece.
Mueller,C.S. and Cranswick,E., (1985). Source parameters from locally recorded aftershocks of the 9 January 1982 Miramichi, New Brunswick, earthquake. Bull. seism. Soc. Am., 75, 337-360.
Papazachos,B.C., Panagiotopoulos,D.G., Tsapanos,T.M., Mountrakis, D.M. and Dimopoulos,G.Ch., (1983). A study of the 1980 summer seismic sequence in the Magnesia region of Central Greece. Geophys. J. R. astr. Soc., 75, 155-168.
Rutter,E.H., (1972). The influence of interstitial water on the rheological behaviour of calcite rocks. Tectonophysics, 14, 13-33.

Savage,J.C. and Wood,M.D., (1971). The relation between apparent stress and stress drop. Bull. seism. Soc. Am., 61, 1381-1388.
Scholz,C.H., (1988). The critical slip distance for seismic faulting. Nature, 336, 761-763.
Sereno,T.J.,Jr., and Bratt,S.R., (1988). Attenuation and detection capability of regional phases recorded at NORESS. Semiannual Report No 3, AFGL-TR-88-0095, Air Force Geophysics Laboratory, Massachusetts 01731.
Sibson,R.H., (1974). Frictional constraints on thrust, wrench and normal faults. Nature, 249, 542-544.
Sibson,R.H., (1982). Fault zone models, heat flow and the depth distribution of earthquakes in the continental crust of the United States. Bull. seism. Soc. Am., 72, 151-163.
Snoke,J.A., Linde,A.T. and Sacks,I.S., (1983). Apparent stress: an estimate of the stress drop. Bull. seism. Soc. Am., 73, 339-348.
Stesky,R.M., Brace,W.F., Riley,D.K. and Robin,P.-Y.F., (1974). Friction in faulted rock at high temperature and pressure. Tectonophysics, 23, 177-203.
Street,R.N., Hermann,R.B. and Nuttli,O.W., (1975). Spectral characteristics of the Lg wave generated by Central United States earthquakes. Geophys. J. R. astr. Soc., 41, 51-63.
Tsubois,C., (1956). Earthquake energy, earthquake volume, aftershock area and strength of the earth's crust. J. Phys. Earth, 4, 63-66.
Wyss,M., (1970). Stress estimates of South American shallow and deep earthquakes. J. Geophys. Res., 75, 1529-1544.
York,D., (1966). Least-squares fitting of a straight line. Can. J. Phys., 44, 1079-1086.